






Parametric identification hybrid metaheuristic-based approach for steel fiber-reinforced concrete using finite element modeling: a comparative study

Wanderlei Malaquias Pereira Junior¹ , Daniel de Lima Araújo² , Eduardo Augusto da Silva Cândido² ,
Fausto Arantes Lobo³ , José Júlio de Cerqueira Pituba¹ 

¹Universidade Federal de Catalão, Faculdade de Engenharia. Av. Dr. Lamartine Pinto de Avelar, Bloco O, Setor Universitário, 75704-020, Catalão, GO, Brasil.

²Universidade Federal de Goiás. Escola de Engenharia Civil e Ambiental. Av. Universitária, Quadra 86, Setor Leste Universitário, 74605-220, Goiânia, GO, Brasil.

³Universidade de Rio Verde, Departamento de Engenharia Civil. Fazenda Fontes do Saber, Bloco IV, Campus Universitário, 75901-970, Rio Verde, GO, Brasil.

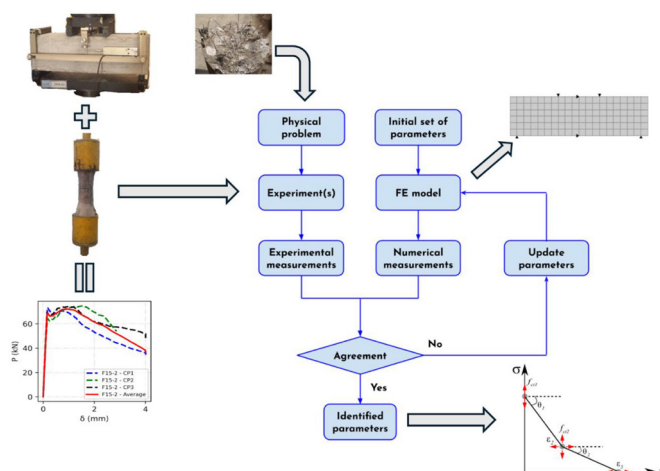
e-mail: wanderlei_junior@ufcat.edu.br, julio_pituba@ufcat.edu.br, dlaraujo@ufg.br, eduardo.augusto@discente.ufg.br, faustoalobo@unirv.edu.br

ABSTRACT

Determining constitutive parameters is essential in nonlinear finite element analysis for structural design. Steel fiber-reinforced concrete (SFRC) is widely used due to its residual strength after cracking. While analytical closed-form solutions are common, inverse analysis using standardized tests provides greater accuracy in capturing the post-peak behavior. This study proposes a hybrid strategy to automate inverse analysis for deriving the tensile stress-strain response of SFRC using four-point bending tests. Hybrid metaheuristic methods enhance search capabilities by combining the strengths of different optimization techniques, often leading to more robust and efficient solutions than traditional methods. By integrating a global search metaheuristic with a local search refiner, for instance, a hybrid approach can effectively explore a vast solution space and then precisely pinpoint the optimal solution within a promising region. Three metaheuristic algorithms were integrated with nonlinear finite element models: Genetic Algorithm (GA), Simulated Annealing (SA), and Differential Evolution (DE). An experimental program with two SFRC mixtures (0.5% and 1.5% steel fiber) tested under flexural and direct tensile loading validated the method. Among the algorithms, the hybrid GA approach achieved the lowest mean square error (MSE). For SFRC with 1.5% fibers (flexural-hardening behavior), the predicted tensile strength aligned well with experimental results. For the 0.5% mixture (flexural-softening behavior), predictions underestimated tensile strength by 27–39% due to crack localization. The proposed hybrid approach improved accuracy in the force-deflection response compared to standalone metaheuristic methods. Overall, the strategy effectively identifies SFRC tensile strength and enhances modeling precision in structural applications.

Keywords: Metaheuristic; Steel Fiber-Reinforced Concrete; Inverse Analysis; Parametric Identification.

GRAPHICAL ABSTRACT



1. INTRODUCTION

The urgency of climate change necessitates the exploration of new possibilities for cementitious materials. Over the past three decades, significant advancements have been made for concrete material, with steel fiber-reinforced concrete (SFRC) emerging as a particularly successful and widely studied variation [1]. The incorporation of steel fibers enhances critical mechanical properties, such as post-crack residual strength [2, 3], energy absorption capacity, and resistance to impacts, making SFRC advantageous for robust and durable civil infrastructure like industrial floors, pavements, and tunnel linings [4–6]. Therefore, the use of SFRC leads to more efficient structures in terms of the amount of materials, which indirectly contributes to the sustainability of civil construction. Despite this progress, accurately predicting the mechanical response of SFRC remains a challenge, and further research is required on topics such as the relationship between stress and crack opening, as well as shear and tensile behavior [7–9].

Compared to other fiber types, the cost of steel fibers is higher than synthetic and natural fibers. Synthetic fibers, such as polypropylene fibers, have great corrosion resistance, making them ideal for aggressive environments. They are lighter, less expensive, and can improve resistance to plastic shrinkage. However, they have lower mechanical performance, offering a smaller enhancement in strength and toughness. Natural fibers are an option from an environmental and economic perspective. They are eco-friendly, biodegradable, renewable, and more affordable than steel and synthetic fibers. Despite these benefits, their mechanical performance is the most limited of these three fibers. Therefore, steel fibers are recommended for structural applications that demand high mechanical performance, while synthetic fibers provide a corrosion-resistant and moderately priced solution. Natural fibers, in turn, serve as a sustainable and economical alternative for less demanding applications [10–13].

The flexural performance of SFRC is directly related to its tensile properties. However, direct tension tests are often impractical for quality control or project implementation in many laboratories. Consequently, the tensile stress-strain relationship is typically determined through inverse analysis of the flexural response from bending tests, a procedure recommended by ACI 544.8R-16 [14, 15]. While various methods exist for this inverse calculation, including finite element analysis, cross-section layer analysis, and iterative solutions [16–19], they frequently rely on trial-and-error techniques. To overcome this limitation, researchers have increasingly employed metaheuristic-based optimization frameworks for inverse analysis problems in structural engineering [7].

Some previous work investigated the applicability of various metaheuristic models for addressing inverse analysis problems within many engineering areas, with the primary focus on parameter identification for material models and structural damage identification. A range of metaheuristic algorithms were evaluated, and the Genetic Algorithm (GA) and the Artificial Bee Colony (ABC) algorithm were effective for the parametric identification of complex concrete damage models. Both methods demonstrated the ability to automate the identification process and achieve a good correlation with experimental data, although GAs occasionally failed to capture strain-softening responses [20].

For structural damage identification, particularly in truss structures and systems monitored by piezoelectric impedance, multi-objective optimization algorithms were featured. The SunFlower Optimization (SFO) algorithm and its multi-objective variant, SFOMO, were accurate to use with both global and local modal responses [21]. However, the better accuracy was observed with the Multi-Objective Simulated Annealing with a Reinforcement Learning Hyper-Heuristic (MOSA/R-HH). This advanced hybrid algorithm consistently surpassed other established methods, including AMOSA, NSGA-II, and MOEA/D, by providing superior solution diversity, completeness, and accuracy, even in the presence of experimental noise [22]. Therefore, while several algorithms demonstrate robust performance, the hybrid and adaptive approaches, such as MOSA/R-HH, offer the most promising and effective solutions for contemporary engineering problems.

This paper proposes a three-step inverse optimization pipeline, driven by metaheuristic algorithms, to determine the tensile stress-strain relationship of SFRC. The methodology integrates data from a four-point bending test with a multi-directional smeared crack model in a nonlinear finite element analysis [23], automated via a custom Python code.

Metaheuristic-based approaches offer distinct advantages for parametric identification in complex material models. Their inherent exploration capabilities are highly effective when initial parameter guesses are unknown, and their Hessian-free nature makes them suitable for optimizing highly nonlinear, discontinuous, or singular functions [24–26]. While alternative methods like machine learning have shown success in other domains, their application here can be hindered by small datasets and a lack of model interpretability [27, 28]. This work leverages a hybrid optimization strategy, combining two search models in three steps, which has shown promise for uniting the advantages of different computational intelligence methods [29–32]. Automating

the parametric identification process replaces inefficient “brute force” methods [33], thereby offering a more robust pathway to improving the performance analysis of structures and contributing to the development of simplified formulations for modern design codes and guidelines [34].

The paper is organized as follows: Section 2 discusses the metaheuristic algorithms used; Section 3 outlines the experimental program and the data-driven pipeline; Section 4 presents and compares the tensile stress-strain curves derived from the experimental program and the inverse optimization; and Section 5 provides the conclusions.

2. RESEARCH SIGNIFICANCE

This study addresses the challenge of determining the tensile stress-strain relationship of steel fiber-reinforced concrete (SFRC), a mechanical property that is still difficult to obtain through direct experimental testing. To overcome the limitations of conventional inverse analysis methods, which often rely on inefficient manual trial-and-error techniques, this work introduces and validates an automated, hybrid optimization pipeline. The methodology integrates data from standardized four-point bending tests with nonlinear finite element analysis, providing a more robust, accurate, and efficient tool for material characterization compared to traditional analytical or standalone metaheuristic methods.

The main contribution is a validated framework that enhances the precision of structural modeling. The results demonstrate that the approach is effective for SFRC exhibiting flexural-hardening behavior, with the hybrid Genetic Algorithm (GA) reaching the best performance and lowest error. Furthermore, the study substantiates the necessity of a fine-tuning step to ensure an accurate force-deflection curve fit and identifies the model’s limitations for concretes with flexural-softening behavior due to crack localization. Thus, this work introduces a robust and automated tool for material characterization that has the potential for automating the process of determining the tensile stress-strain relationship of SFRC.

However, it is emphasized that determining the mechanical properties of SFRC through inverse analysis presents several complexities. The method is intrinsically dependent on the adopted numerical model. If the model cannot adequately capture the material’s cracking phenomena and post-peak behavior, the identified parameters may lack real physical meaning, even if they provide a good fit between the experimental and numerical curves. The choice of test setup is fundamental for the correct identification of material parameters. Tests that do not represent the stress field of the element to be designed can lead to erroneous results. Additionally, the specimen’s size and geometry can influence the distribution and orientation of the fibers, which may also differ from the distribution in the final structural element.

3. METAHEURISTIC ALGORITHMS

3.1. Genetic Algorithm

The Genetic Algorithm (GA) functions as a search metaheuristic, drawing inspiration from Charles Darwin’s evolutionary theory. This algorithm reflects the process of natural selection, where the fittest individuals are selected for reproduction to produce offspring, forming the next generation [30]. The Genetic Algorithm was developed by HOLLAND [35].

According to Darwin’s theory of evolution, individuals with characteristics that are superior to other individuals will have a greater chance of survival. Therefore, their superior characteristics will be transferred to the next generation. On the other hand, the second part of Darwin’s theory states that, when multiplying, an event can occur that changes the characteristics of the children. If these changes benefit the children, it will increase the probability of survival of those children [36, 37].

In the GA, the new populations are produced by the iterative use of genetic operators on agents present in the population. The genetic operators considered in this algorithm are [38]: (a) selection, (b) crossover, and (c) mutation.

In this paper, we applied a roulette wheel selection operator; see details in KRAMER [39]. We used a linear strategy and a BLX- α strategy in the crossover process. In a linear crossover of two parent points, p_0 and p_1 , three new points are generated (offspring); see Eq. (1) to Eq. (3). In these equations, k is the k^{th} component of the design variable vector, and t is a current iteration.

$$ch_{a,k} = 0.50 \cdot p_{0,k}^t + 0.50 \cdot p_{1,k}^t \quad (1)$$

$$ch_{b,k} = 0.50 \cdot p_{0,k}^t + 0.50 \cdot p_{1,k}^t \quad (2)$$

$$ch_{c,k} = 0.50 \cdot p_{0,k}^t + 0.50 \cdot p_{1,k}^t \quad (3)$$

The best of the three points (offspring ch_a , ch_b and offspring ch_c) are selected; see Eq. (4).

$$\min(of(\mathbf{ch}_a), of(\mathbf{ch}_b), of(\mathbf{ch}_c)) \Rightarrow x^{t+1} = \text{best}(\mathbf{ch}_a, \mathbf{ch}_b, \mathbf{ch}_c) \quad (4)$$

In Blend crossover (BLX- α), from the two parent points, p_0 and p_1 , two new points are generated (offspring); see Eq. (5) to Eq. (7). In these equations, k is the k^{th} component of the design variable vector, and α is a uniformly distributed random number, such that $\alpha \in [0,1]$; t is the current iteration.

$$ch_{a,k} = \min(p_{0,k}^t, p_{1,k}^t) - \alpha \cdot d_k^t \quad (5)$$

$$ch_{b,k} = \max(p_{0,k}^t, p_{1,k}^t) - \alpha \cdot d_k^t \quad (6)$$

$$d_k^t = |p_{0,k}^t - p_{1,k}^t| \quad (7)$$

The best of the two points (offspring ch_a and offspring ch_b) are selected; see Eq. (8).

$$\begin{aligned} \min(of(\mathbf{ch}_a), of(\mathbf{ch}_b)) &\Rightarrow x^{(t+1)} \\ &= \text{best}(\mathbf{ch}_a, \mathbf{ch}_b) \end{aligned} \quad (8)$$

The mutation process uses a hill-climbing algorithm to move the particle [40]. The iterative procedure continuously improves the solution until the best solution is attained. The process consists of generating random neighbors for the current solution, according to Eq. (9), where N indicates a Gaussian or uniform distribution, where the mean x^t is the current solution and cov is the coefficient of variation input by the user. In this equation, k is the k^{th} component of the design variable vector x , and t is a current iteration.

$$x_{i,k}^{t+1} \sim N(x_{i,k}^t, \sigma) \quad (9)$$

$$\sigma = x_{i,k}^t \cdot \frac{cov}{100} \quad (10)$$

3.2. Simulated annealing algorithm

The Simulated Annealing method was introduced by KIRKPATRICK *et al.* [41] in 1983 [42]. This algorithm was inspired by the annealing process of metals during the manufacturing process. The Simulated Annealing model is based on the generation of random neighbors from a starting point, similar to the Monte Carlo method.

In the Simulated Annealing algorithm, the acceptance of the new solution is given by a criterion that compares the energy of the system given by Eq. (11). In this algorithm, the values of E_i are relative to the value of the objective function, i.e., $E_i = of_i$.

$$\Delta E = E_{new} - E_{cur} \quad (11)$$

E_{new} is the value of the objective function for the newly generated neighbor, and E_{cur} is the value of the objective function for the current particle.

The solution will be accepted if $E_{cur} > E_{new}$ ($P(\Delta E, T) = 1$). For solutions of type $E_{cur} < E_{new}$, acceptance follows a certain probability, given by Eq. (12).

$$P(\Delta E, T) = e^{\frac{-\Delta E}{T}} \quad (12)$$

At the end of the algorithm, the entire temperature is updated by a geometric decay, where α is the cooling temperature adjustment. In this paper, $\alpha = 0.90$ was used.

$$T^{t+1} = \alpha \cdot T^t \quad (13)$$

3.3. Differential evolution algorithm

Differential Evolution (DE) is a global optimization technique introduced in the late 1990s by STORN and PRICE [43]. DE works in two phases: initialization and evolution. In the first phase, population is generated randomly, and, in the second phase (evolution), the generated population goes through mutation, crossover and selection processes, which are repeated until the termination criteria are met [44].

Mutation specifies how a DE makes small random changes in the individuals in the population to create mutated children (v). Mutation provides genetic diversity and enables the DE algorithm to search for a broader space. A mutant vector is generated using a popular strategy, $\text{rand}/1$ [45]. In this strategy, x_r is a random vector selected from the population, f is the scale factor that controls the magnitude of the difference vector, and k is the k^{th} component of the design variable vector.

$$v_k = x_{r_0,k}^t + f \cdot (x_{r_1,k}^t - x_{r_2,k}^t) \quad (14)$$

In the equations above, r_0 , r_1 and r_2 are exclusive integer numbers ranging from 1 to the number of the population, and they are different from the current solution i .

After mutation, crossover is executed based on the current solution (x_i^t) and mutation solution (v) to generate trial vectors (u). The binomial crossover operator is mostly used, and it is defined as [45], where p_c is the crossover rate ($p_c \in [0,1]$).

$$u_k = \begin{cases} v_k & \text{if } \text{rand}(0,1) \leq p_c \\ x_{i,k}^t & \text{otherwise} \end{cases} \quad (15)$$

Once the trial vector is produced, the selection operator will make a comparison between the target vector x_i^t and the trial vector u and choose the superior one to survive to the next generation. The selection operator is performed as below [45]:

$$x_i^{t+1} = \begin{cases} x_i^t & \text{if } f(x_i^t) \leq f(u) \\ u_k & \text{otherwise} \end{cases} \quad (16)$$

4. MATERIALS AND METHODS

4.1. Experimental program

To validate the proposed hybrid optimization strategy, two steel fiber-reinforced concrete (SFRC) mixtures were developed in this investigation. The experimental program was designed with one mixture exhibiting flexural-softening behavior and another exhibiting flexural-hardening. From previous research [46], a steel fiber volume fraction of 0.5% (F-05-2) was adopted to induce flexural-softening, while a 1.5% volume fraction (F-15-2) was chosen to achieve flexural-hardening. A plain concrete mixture without fibers (F-00-02) was included as a

Table 1: Mixture proportion of concrete (kg/m³).

MIXTURE	CEMENT	WATER	SILICA FUME	NATURAL SAND	ARTIFICIAL SAND	COARSE AGGREGATE	STEEL FIBERS	SUPERPLASTICIZER ADMIXTURE	WATER / CEMENT RATIO
F-00-2	483	182	19	379	350	836	0	9.65	0.38
F-05-2	483	182	19	379	350	836	39.25	10.16	0.38
F-15-2	483	182	19	379	350	836	117.75	11.18	0.38

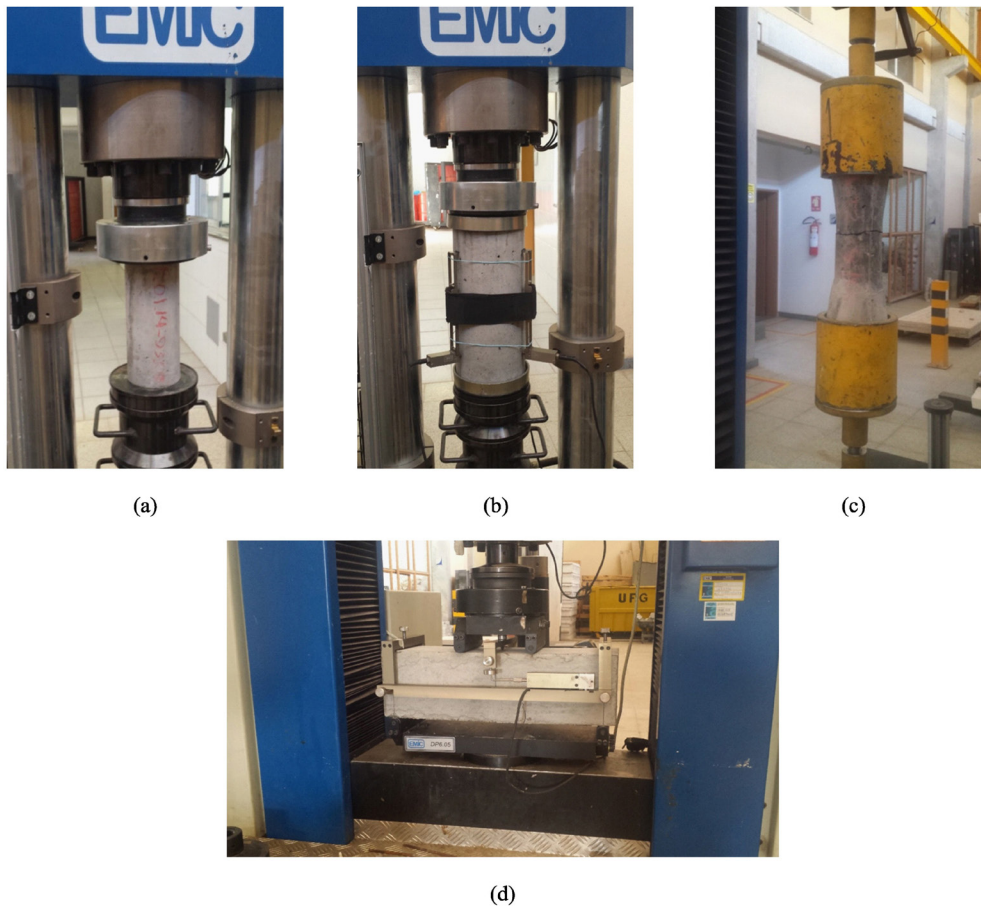


Figure 1: Test apparatus. (a) Compressive strength test; (b) modulus of elasticity test; (c) axial tensile strength test; (d) beam with four-point loading.

reference. Therefore, if the proposed hybrid optimization model accurately represents the stress-strain relationship for both SFRC mixtures, the strategy's effectiveness can be extended to other SFRC applications with fiber volumes within the studied range.

Portland cement, with 6 to 10% limestone filler, and coarse aggregate obtained from crushed stone were used. The maximum dimension of coarse aggregate was 12.5 mm. Additionally, fine aggregate consisted of natural sand obtained from the river and artificial sand, or limestone filler, obtained by crushing rocks were used. The steel fibers used had hooked ends and a circular cross-section that was 35 mm long and 0.55 mm wide. They had an aspect ratio of 64 and a minimum tensile strength of 1150 MPa. The matrix without steel fibers was previously characterized, achieving an average compressive strength of 63 MPa after 28 days. Table 1 shows the quantity of materials used to produce F-05-2 and F-15-2 mixtures [46].

All specimens were produced in steel molds, and the consolidation of the SFRC with 1.5% steel fibers was performed using a vibrating table, since it presented a slump of 15 mm, despite the matrix presenting self-consolidating behavior with a flow of 567 mm. The mixtures without fibers and with 0.5% steel fibers were compacted manually, as they showed slump between 208 and 230 mm. The air content in the mixtures with and without fibers varied between 0.8% and 1.5%. All specimens were kept in a humid chamber at a temperature of 22 ± 2 °C and humidity greater than 95%, remaining in this condition until the date of the test.

SFRC mixtures were characterized to determine their compressive strength, modulus of elasticity, tensile strength, and force-deflection curve from beams subjected to four-point loading. The compressive strength was determined according to the Brazilian standard ABNT NBR 5739 [47]. Six cylindrical specimens, measuring 100×200 mm, were tested for each SFRC mixture in this study (Figure 1(a)). The modulus of elasticity was determined in accordance with the Brazilian standard ABNT NBR 8522 [48]. Three cylindrical specimens (measuring 150×300 mm) were used for each SFRC mixture in this study (Figure 1(b)).

The test to determine the flexural strength of the SFRC and the residual strength was performed based on the ASTM C1609 standard [49]. For this test, three prismatic specimens, with dimensions of $150 \times 150 \times 500$ mm and a span (L) of 450 mm, were used with four-point loading (Figure 1(d)). The testing was conducted in

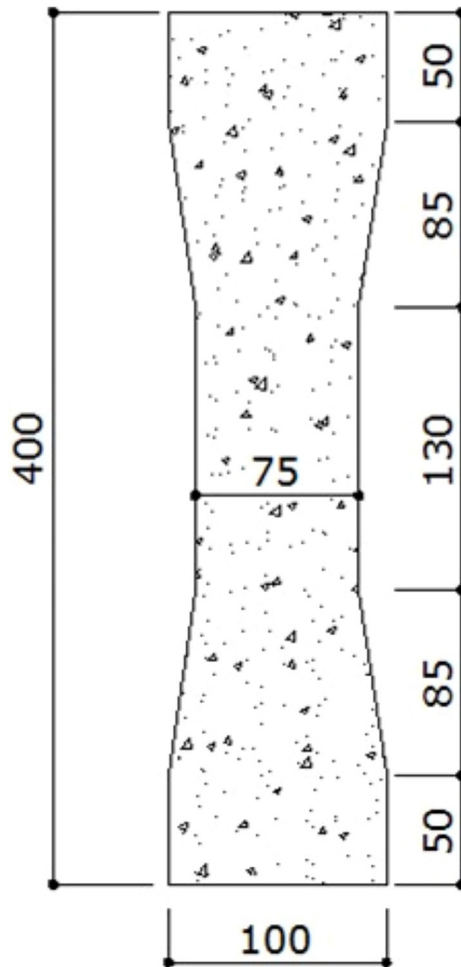


Figure 2: Dimensions of the cylindrical specimen used in the direct tensile test (mm).

a closed-loop manner, utilizing an electromechanical testing system to control the vertical displacement of the specimen. This was recorded by two deflectometers, with a resolution of 0.001 mm. The displacement rate used in the test was 0.10 mm/min until the maximum vertical displacement of $L/900$ was reached and 0.30 mm/min until the maximum vertical displacement of $L/150$ was reached. This setup was chosen instead of the flexural setup recommended by Model Code 2010 [50] because the ASTM C1609 [49] setup did not have an initial crack. Therefore, the regular finite element mesh can be used in hybrid optimization, and the stress-strain curve can be obtained directly without setting up the crack bandwidth in the finite element software.

Besides the bending test, the SFRC was characterized to determine its tensile strength (Figure 1(c)). Three cylindrical specimens, measuring 100×400 mm, were tested with a smooth reduction in the diameter of the cross-section to 75 mm at the mid-height. Figure 2 shows the size of the specimen used for the direct tensile test. This test was conducted to determine the tensile strength of the concrete, which is one of the output data in the inverse analysis approach. It is a mechanical property not commonly determined in other works presented in literature and is used to validate the output of the proposed hybrid strategy in this study.

The specimens were attached to the testing machine using two devices developed by the authors for this work. The fixing device consists of a main part formed by a steel cylinder, internally containing a spring with steel metal teeth that allow the test cup to be locked as the value of the traction load increases. It also features threaded parts and labeled pins for allowing the specimen to rotate, as well as solid steel bars for fixing it to the testing machine. A device was attached to each end of the test piece, ensuring that the test scheme was double pinned.

4.2. Proposal for inverse analysis approach

Figure 3 shows the optimization pipeline for the inverse analysis approach considering a finite element model. In this work, a hybrid approach was used to predict parameters in the tensile stress-strain curve of the SFRC

(updated parameters phase). This same pipeline was used in research carried out by this research group; see PEREIRA JUNIOR *et al.* [51, 52].

In this study, the objective function is given by Eq. (17), and it represents the mean square error (MSE) measurement (Loss). MSE was adopted as the objective function due to its widespread use as a standard performance metric for regression problems in machine learning and optimization. It quantifies the average of the squared differences between predicted and actual values, penalizing larger errors more heavily. This results in a smooth, differentiable, and computationally efficient loss surface, making it particularly suitable for gradient-based or evolutionary optimization methods. Moreover, this characteristic makes MSE especially appropriate for problems where large deviations from the true value are undesirable [53].

$$MSE = \frac{1}{n} \sum_{i=1}^n (y_{i,pred} - y_{i,true})^2 \quad (17)$$

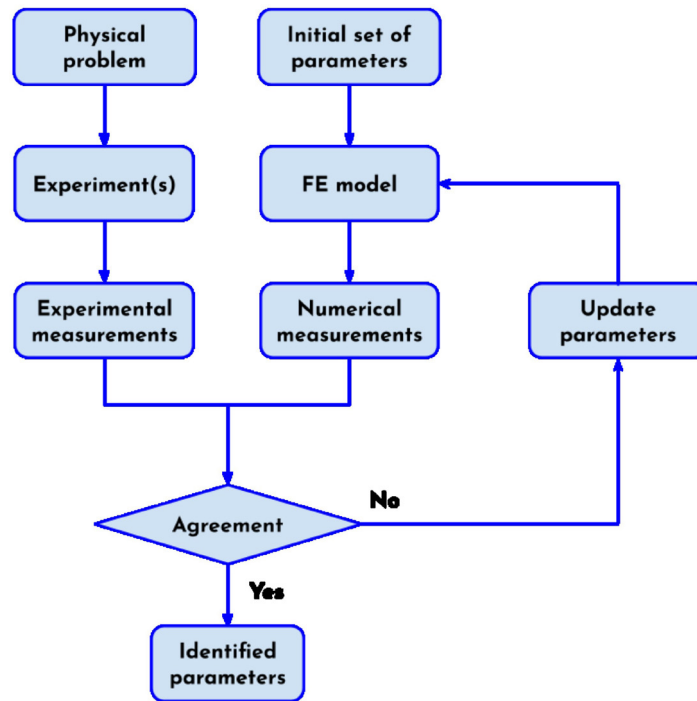


Figure 3: Inverse optimization pipeline.

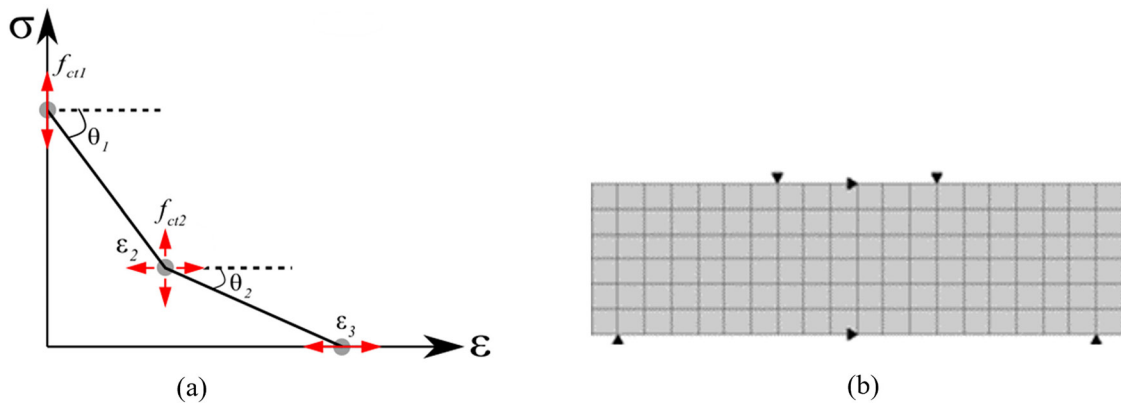


Figure 4: The bilinear softening curve (a) and mesh refinement in FEM analysis (b).

In this process, $y_{i,true}$ represents the vector of observations, $y_{i,pred}$ represents the vector of predictions, and n represents the number of points.

The finite element model was solved using the DIANA FEA package [23], version 10.1. The multi-directional fixed crack model with a smeared crack approach was used. Once the tensile strength of the material is reached, the user can select the softening behavior of the material. In this study, strain softening behavior with a bilinear stress-strain curve was selected, as illustrated in Figure 4(a). Although the trilinear curve can be used by other researchers to simulate the SFRC, the bilinear tension softening curve is sufficient to represent the load-deflection curves of beams with SFRC [54]. The stress-strain parameters f_{ct1} , f_{ct2} , ε_2 and ε_3 represent design variables in the optimization problem and are the outputs of the automated inverse analysis approach.

The finite element analysis was performed using an isoparametric element with quadratic interpolation in a plane stress state. Based on the mesh refinement analysis, a regular mesh, comprising 25×25 mm elements, was selected (Figure 4(b)). The mesh refinement in plain concrete modeling with a smeared crack approach is dependent on the energy dissipated in tension, which also depends on the aggregate size. This mesh refinement was chosen for further analysis because it is twice the maximum aggregate size used in the mixture of SFRC, which approximately matches the minimum ratio suggested by other research [55, 56]. Furthermore, it is identical to the size utilized in other works [17]. However, due to the stress-strain curve and multi-directional fixed crack model being used in the analysis, the fracture energy and crack bandwidth were not informed in the software. Therefore, these parameters are not determined in this inverse analysis approach. The analysis was conducted using displacement control at the test load points. The boundary conditions were established to guarantee the model's symmetry. Regarding the resolution of the nonlinear system, the Quasi-Newton method of the BFGS type was employed, with a convergence norm in energy and tolerance of 10^{-3} .

The optimization process in the numerical measurements presented in Figure 3 involved three steps. Figure 5 details the hybrid optimization pipeline for the inverse approach. In this study, this hybrid process was divided into three steps.

In the first step, the crude Monte Carlo algorithm was used to sample a set of variables, agreeing with the geometric constraints in the tensile model. Two hundred fifty (250) samples were generated, and this number was selected because tests demonstrated that increasing it produces more quantity feasible tension softening curves. However, in the second phase, there was no improvement in MSE measurement optimization.

The side constraints used in the first phase of the inverse analysis are proposed in Eq. (18) to Eq. (25). The parameter $f_{m,ref}$ is an initial estimate of the tensile strength. In this study, this value is the experimental tensile strength. The inequalities (24) and (25) were defined so that the resulting softening curve always met the format

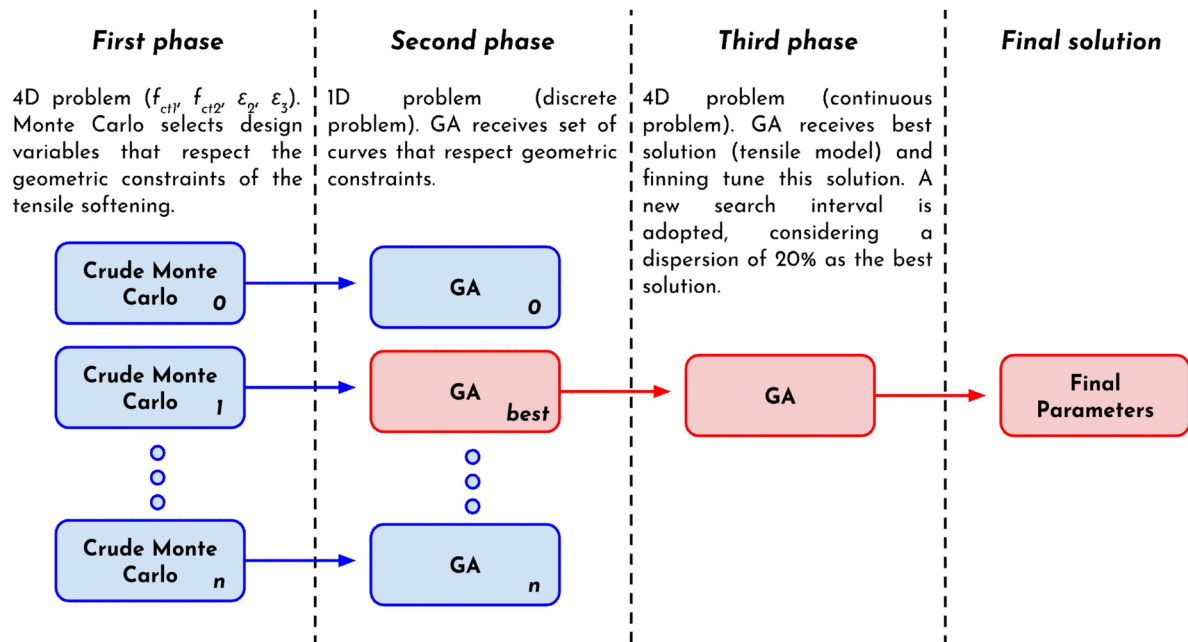


Figure 5: Hybrid optimization pipeline proposed in this work for the inverse analysis approach (n repetitions GA example).



Figure 6: The failure of the specimens from the direct tensile test and the number of fibers (N_f) in the fractured plane. (a) Mixture F-15-2 ($N_f = 64.7 \pm 15.2$); (b) mixture F-05-2 ($N_f = 24.3 \pm 10.0$).

shown in Figure 6. Therefore, the angle θ_1 , which represents the stress decay rate in the first section of the curve, will always be smaller than the flexural modulus of elasticity (E_f), and the angle θ_1 will always be smaller than the angle θ_1 .

$$0.50 \cdot f_{tm,ref} \leq f_{ct1} \leq 2.00 \cdot f_{tm,ref} \quad (18)$$

$$0.50 \cdot f_{tm,ref} \leq f_{ct2} \leq f_{tm,ref} \quad (19)$$

$$0.0005 \leq \varepsilon_2 \leq 0.0583 \quad (20)$$

$$\begin{cases} 0.005 \leq \varepsilon_3 \leq 1000.00 & \text{for F-15-2 dataset} \\ 0.005 \leq \varepsilon_3 \leq 10.00 & \text{for F-05-2 dataset} \end{cases} \quad (21)$$

$$0.1 \cdot f_{ct1} \leq f_{ct2} \quad (22)$$

$$\varepsilon_2 \leq \varepsilon_3 \quad (23)$$

$$\theta_1(f_{ct1}, f_{ct2}, \varepsilon_2) \leq E_f \quad (24)$$

$$\theta_1(f_{ct2}, f_{ct3}, \varepsilon_2, \varepsilon_3) \leq \theta_1(f_{ct1}, f_{ct2}, \varepsilon_2) - f_{ct3} \text{ equal zero in this modeling} \quad (25)$$

The first phase guarantees that the problem will have design variables (f_{ct1} , f_{ct2} , ε_2 and ε_3) that always respect the tension-softening criteria. Therefore, creating a restricted optimization problem in the second phase is unnecessary, which would make the optimization process more complex.

In the first phase, the crude Monte Carlo algorithm generated a list of solutions. All feasible solutions are evaluated in the second phase, considering a one-dimensional, unconstrained problem. At this stage, the optimization problem is treated as a discrete problem, where the four parameters f_{ct1} , f_{ct2} , ε_2 and ε_3 assemble the shape of the tension softening curve. Therefore, the discrete optimization procedure will try to find the best shape of the curve. In this phase, the design variable is the shape of tension softening. Thirty runs were applied in this phase. Phases one and two can be called the “Exploration Phase” because they try to select the best shape for the tension-softening curve.

In the third phase, the best second-phase output underwent fine-tuning. The problem was treated as a continuous problem; new side constraints were created. $f_{ct,best}$ and ε_{best} correspond to the tension softening parameters of the best shape selected in the second phase; see Eq. (26) to Eq. (29). Thirty runs were applied in this phase, and this phase can be called the “Exploitation Phase”.

$$0.80 \cdot f_{ct1,best} \leq f_{ct1} \leq 1.20 \cdot f_{ct1,best} \quad (26)$$

$$0.80 \cdot f_{ct2,best} \leq f_{ct2} \leq 1.20 \cdot f_{ct2,best} \quad (27)$$

$$0.80 \cdot \varepsilon_{2,best} \leq \varepsilon_2 \leq 1.20 \cdot \varepsilon_{2,best} \quad (28)$$

$$0.80 \cdot \varepsilon_{3,best} \leq \varepsilon_3 \leq 1.20 \cdot \varepsilon_{3,best} \quad (29)$$

Tables 2 to 4 describe the settings of the optimization algorithm used in this study.

The choice of algorithms in this study was guided by their suitability to the problem characteristics and their established performance in similar applications. While numerous algorithms could have been considered, the selected methods offer a balanced trade-off between accuracy, interpretability, and computational efficiency. Moreover, these algorithms are widely used and well-studied in the literature, which facilitates reproducibility

Table 2: GA setup.

ALGORITHM	POPULATION	ITERATIONS	CROSSOVER RATE (%)	CROSSOVER MODEL	MUTATION RATE (%)	COV (%)
Discrete GA	10	100	85	blx- α	15	15
Continuous GA	10	30	85	linear	15	5

cov - Coefficient of Variation in mutation process.

Table 3: SA setup.

ALGORITHM	POPULATION	ITERATIONS	INITIAL TEMPERATURE	TEMPERATURE UPDATE	MUTATION RATE (%)	COV (%)
Discrete SA	10	100	100	Geometric / 0.90	100	15
Continuous SA	10	30	100	Geometric / 0.90	100	5

cov - Coefficient of Variation in mutation process.

Table 4: DE setup.

ALGORITHM	POPULATION	ITERATIONS	CROSSOVER RATE (%)	SCALE FACTOR (F)
Discrete DE	10	100	90	0.85
Continuous DE	10	30	90	0.85

and comparison. A comprehensive benchmark of all available methods is beyond the scope of this work; instead, our focus is on demonstrating the effectiveness of the selected approaches within the context of the proposed framework.

5. RESULTS

This section initially presents the results obtained from the experimental program. The results of the automated proposed inverse analysis approach are also presented; that is, the bilinear tensile stress-strain curve for both mixtures of SFRC.

5.1. Mechanical properties of SFRC

Table 5 presents the mechanical properties of the two SFRC mixtures, as well as the matrix without the inclusion of steel fibers (F-00-2). It should be noted that the variation in the volume of steel fibers did not influence either the average compressive strength or the value of the modulus of elasticity. When performing an analysis of variance with $\alpha = 0.05$, it is concluded that these properties were not significantly influenced by the variation in the volume of steel fibers. Therefore, the properties of plain concrete can be used for these parameters.

Figure 6 shows the failure aspect of the specimens after the direct tensile test, which failed in the reduced section. It also shows the arrangement and number of fibers in the fracture plane. The fracture plane was normal to the axis of the specimen, but there were some ramifications when the mixture had 1.5% steel fibers. According to Table 5, there was no increase in the tensile strength of the matrix with the addition of steel fibers, which was confirmed by the analysis of variance with $\alpha = 0.05$. Despite an increase of almost 170% in the number of fibers in the fracture plane in the mixture with 1.5% steel fibers, no increase in tensile strength was observed with an increase in the volume of steel fibers added to the concrete.

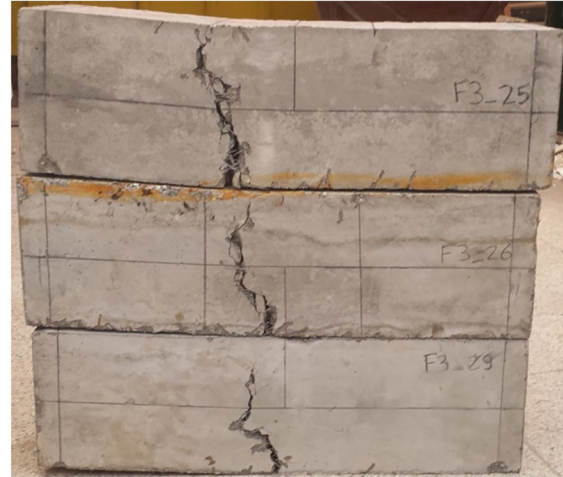
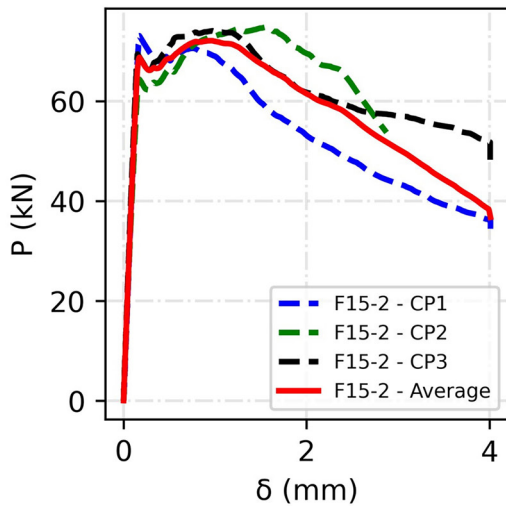
Figure 7 presents the load versus displacement curves for each specimen from the bending test with four-point loading, as well as the average curve for each SFRC mixture. It should be noted that the mixture with 1.5% of fibers achieved a peak load 28% greater than the mixture with 0.5% of added fibers. Moreover, the mixture with 1.5% of fibers presented a flexural-hardening behavior, since the ultimate force was greater than the force relative to cracking the matrix. Figure 7 also shows the crack pattern of the specimens, which indicates that the crack was inclined and branched with 1.5% fibers. On the other hand, the crack in the specimen with 0.5% of steel fibers was vertical and without branches, which justified the lower flexural strength shown in Table 5. The mixture F-05-2 presented a flexural-softening behavior after the cracking of the matrix.

It is important to mention that the modulus of elasticity determined from compression in cylindrical specimens (Table 5) is normally higher than the flexural stiffness of the beam. The lower value of flexural stiffness is justified by the fact that the specimen is subjected to both compression and tensile stresses during bending. For example, the tensile modulus of elasticity measured in tests from SFRC with 1.5% of hooked fibers is up to 34% lower than the modulus of elasticity measured in compression [57]. This difference is because in concrete under tensile stress, the greater stiffness of the aggregates has less influence on the deformation of the composite, while the stiffness of the hydrated cement paste has the greatest influence on the stiffness of the composite. On the other hand, the compressive modulus of elasticity is influenced by the modulus of elasticity of the paste and the coarse aggregate.

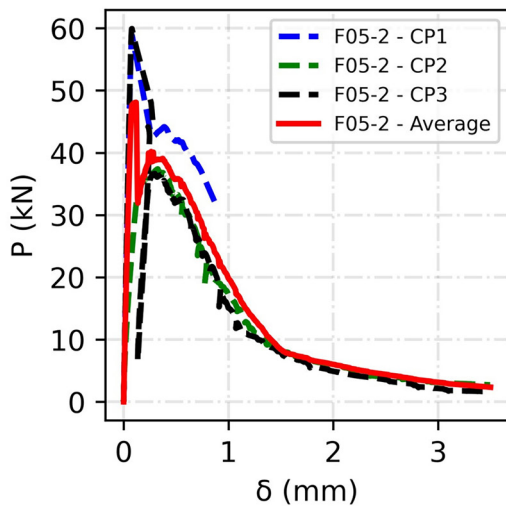
Table 5: Mechanical properties of concrete.

MIXTURE	V_f (%)	f_{cm} (MPa) (μ/σ)	$f_{tm,ref}$ (MPa) (μ/σ)	$f_{tm,f,ref}$ (MPa) (μ/σ)	E_{cm} (GPa) (μ/σ)
F-00-2	0.0	65.08/4.73	4.13/0.90	—	39.04/0.74
F-15-2	1.5	68.74/8.57	3.93/1.02	9.89/0.11	40.39/1.84
F-05-2	0.5	65.98/5.77	4.33/0.58	7.70/0.43	37.62/1.20

Mean (μ) and standard deviation (σ), V_f is volume of steel fibers; f_{cm} is compressive strength of concrete; $f_{tm,ref}$ is tensile strength of concrete; $f_{tm,f,ref}$ is flexural strength of concrete; E_{cm} is modulus of elasticity of concrete.



(a)



(b)

Figure 7: Results of the bending tests (force-displacement) with four-point loading. (a) mixture F-15-2; (b) mixture F-05-2.

To obtain a correct flexural stiffness of the SFRC under bending, a simply supported beam subjected to two vertical loads, representing a bending test with four-point loading, was modeled in the DIANA software. The modulus of elasticity in the model has been varied such that the load-displacement curve of the model agreed well with the elastic response of the experimental results. The value obtained from this analysis, using the mesh refinement presented in Figure 4(b), was 23.28 GPa. This value was about 60% of the modulus of elasticity obtained from the compression test using a cylindrical specimen and is used for all inverse analysis.

5.2. Inverse analysis of SFRC with $V_f = 1.50\%$

Figure 8 shows the results of the first phase optimization procedure, which involved thirty repetitions. The best result obtained in this procedure was a loss of 8.13 kN (the MSE value in the Genetic Algorithm). Table 6 shows statistical analysis. The GA algorithm also presented the slightest standard deviation of about 30 repetitions.

Figure 8 also shows the behavior of the best particle across all runs. In the GA algorithm, seven repetitions reached a loss value of less than 15 kN, totaling 23.3% of the repetitions. In the SA algorithm, just four repetitions (13.3%) reached a loss value of less than 15 kN and in the DE algorithm, six repetitions (20.0%) reached a less-than-reference loss.

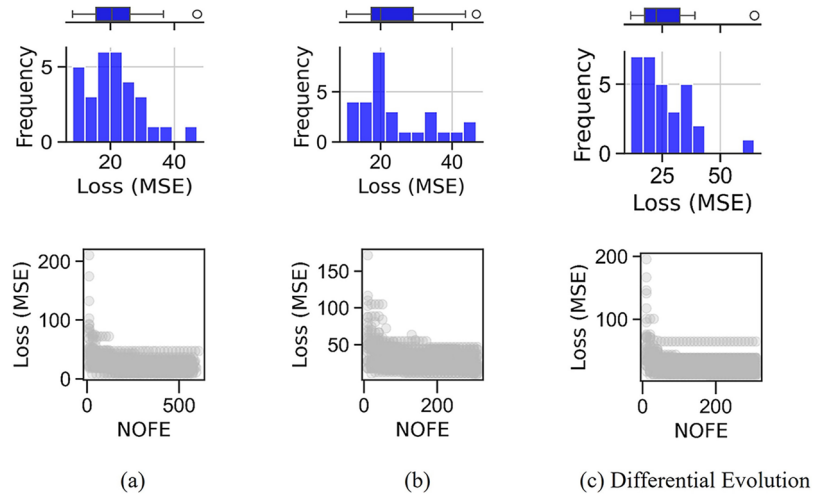


Figure 8: Performance of 30 runs of the Genetic Algorithm and loss versus number of objective function evaluations (NOFE) of all repetitions: (a) Genetic Algorithm; (b) simulated annealing; (c) differential evolution.

Table 6: Statistical analyses of all algorithms after thirty runs.

ALGORITHM	BEST LOSS (kN)	WORST LOSS (kN)	μ (kN)	σ (kN)
GA	8.13	47.12	21.47	8.62
SA	10.44	46.77	23.51	10.16
DE	11.46	64.72	25.25	11.53

μ is mean, and σ is standard deviation.

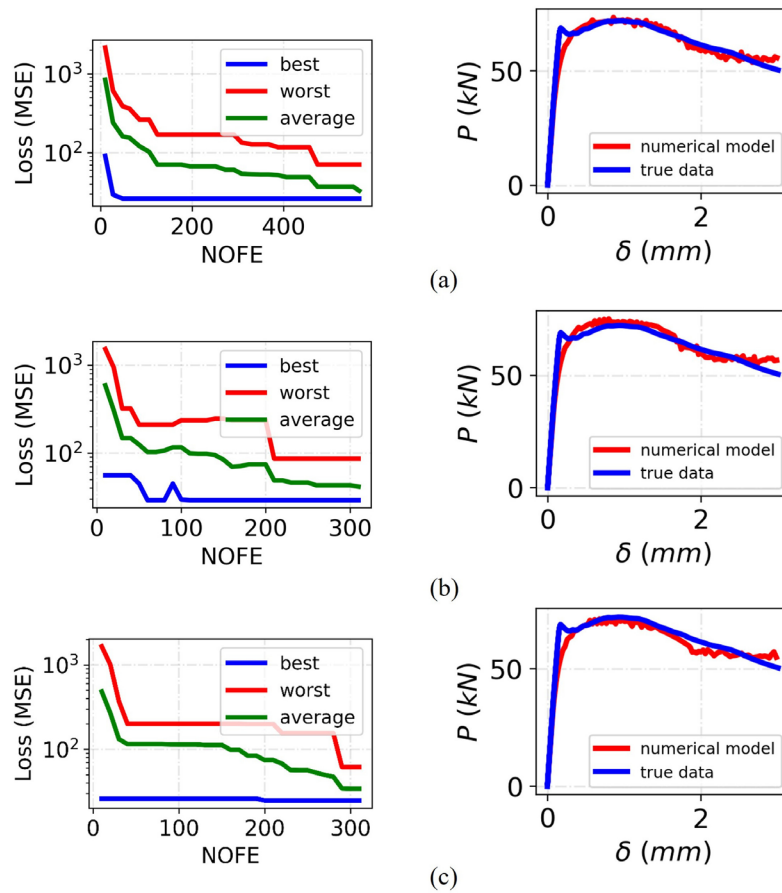


Figure 9: Loss (MSE) versus number of objective function evaluations (NOFE) and load-displacement path for SFRC with 1.5% of fibers: (a) GA results; (b) SA results; (c) DE results.

Table 7: Best parameters of each algorithm for SFRC with 1.50%.

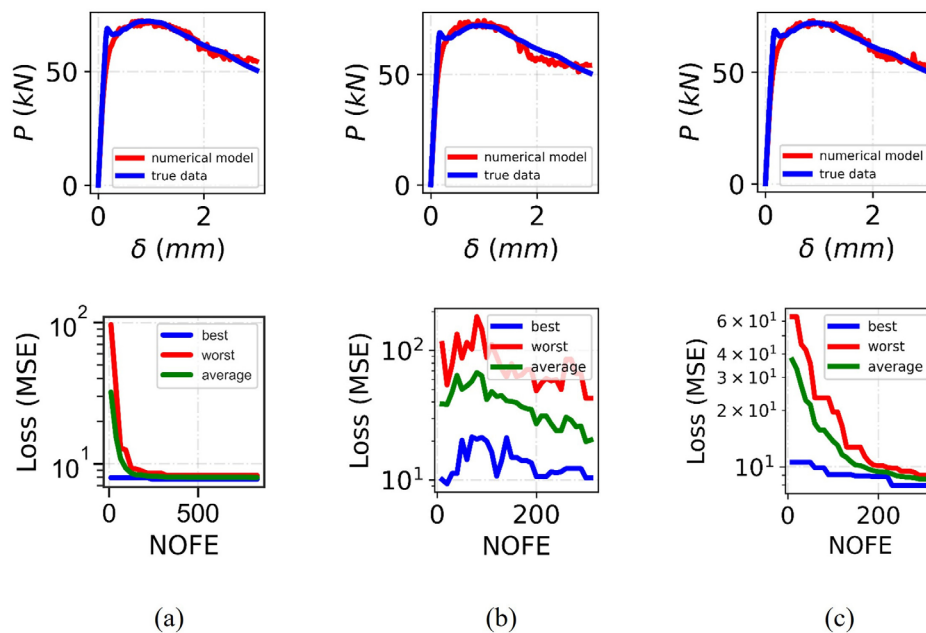
ALGORITHM	f_{ct1} (MPa)	f_{ct2} (MPa)	ε_2 (mm/mm)	ε_3 (mm/mm)
GA	4.021	2.409	0.024	683.673
SA	4.134	2.439	0.023	315.990
DE	3.943	2.335	0.022	124.295

Figure 9 shows behavior around the best repetition, and Table 7 presents the best parameters of each algorithm. It is possible to verify that the algorithms reach convergence on the optimal solution before 100 objective function evaluations. In the GA metaheuristic, the difference in the loss value between the best solution (8.13 kN) and the average solution (32.75 kN) is approximately 302%.

After the discrete optimization process, the best solution was inserted in the third phase (the fine-tuning process). Figure 10 shows a numerical model compared with the experimental result and convergence process. Table 8 shows the best parameters after fine-tuning. It can be seen that the SA optimization algorithm could not improve the solution presented in Table 7. The GA and DE algorithms improved the prediction response by 4.31% and 30.54%, respectively.

The three algorithms achieved a tensile strength (f_{ct1}) of approximately 4 MPa. This value is practically equal to the experimental average tensile strength obtained from the test, which is 3.93 MPa for this mixture. This confirms the ability of the metaheuristic algorithms to estimate the correct tensile strength of the SFRC from an inverse analysis approach. Furthermore, they confirm the test results that indicate that adding steel fibers to this mixture did not increase the tensile strength but only influenced the residual strength after the cracking of the matrix. Despite the flexural hardening observed during the beam test, the inverse analysis approach indicated that the SFRC containing 1.5% steel fibers displayed a tension-softening response.

Using the inverse analysis process with the standard GA algorithm, without the proposal presented in this study, convergence of the optimization process was obtained after 40 generations. The processing time to obtain

**Figure 10:** Load-displacement path and loss (MSE) versus number of objective function evaluations (NOFE) for SFRC with 1.5% of fibers: (a) Genetic Algorithm; (b) simulated annealing; (c) simulated annealing.**Table 8:** Best parameters after fine-tuning.

ALGORITHM	f_{ct1} (MPa)	f_{ct2} (MPa)	ε_2 (mm/mm)	ε_3 (mm/mm)	IMPROVEMENT OF?
GA	3.946	2.409	0.0240	701.913	Yes. Final value: 7.78 kN
SA	4.078	2.345	0.0233	270.494	No. Final value: 10.32 kN
DE	3.963	2.315	0.0266	135.034	Yes. Final value: 7.96 kN

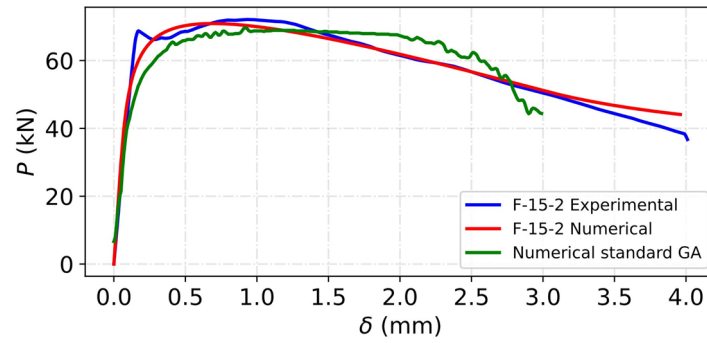


Figure 11: Load-displacement curve by traditional GA algorithm optimization and closed-form solution proposed in MOBASHER *et al.* [58] for SFRC with 1.5% of fibers.

the average curve shown in Figure 11 was over 11 hours for an initial population of 10 individuals and up to 60 hours for an initial population of 50 individuals. The use of the hybrid optimization pipeline proposed in Figure 5 provided a better fit to the experimental force-displacement curve, as can be seen in Figure 10(a).

Using the trial-and-error procedure with a closed-form solution proposed in MOBASHER *et al.* [58], adopting a tensile strength value of $f_{ct1} = 3.96$ MPa and a modulus of elasticity $E_f = 23.28$ GPa, the results of residual stress f_{ct2} and strain ε_2 are 1.58 MPa and 0.029, respectively. The value of residual stress f_{ct2} obtained from the closed-form solution is approximately 34% lower than that obtained from the inverse analysis approach in this study. However, strain ε_2 agrees well with both analysis procedures. The strain ε_3 presented in Table 7 cannot be compared to the closed-form solution, as the load during the bending test did not reach a zero value. Figure 11 shows the load-deflection curve obtained from the closed-form solution proposed in MOBASHER *et al.* [58], which agrees well with the results of the experiments until a displacement of 3 mm.

5.3. Inverse analysis of SFRC with $V_f = 0.50\%$

In this section, only the Genetic Algorithm is applied to experimental results, as it obtained the best performance for concrete with 1.5% steel fibers. Figure 12(a) shows the results after the second step of this pipeline, and Figure 12(b) shows the results after the fine-tuning process.

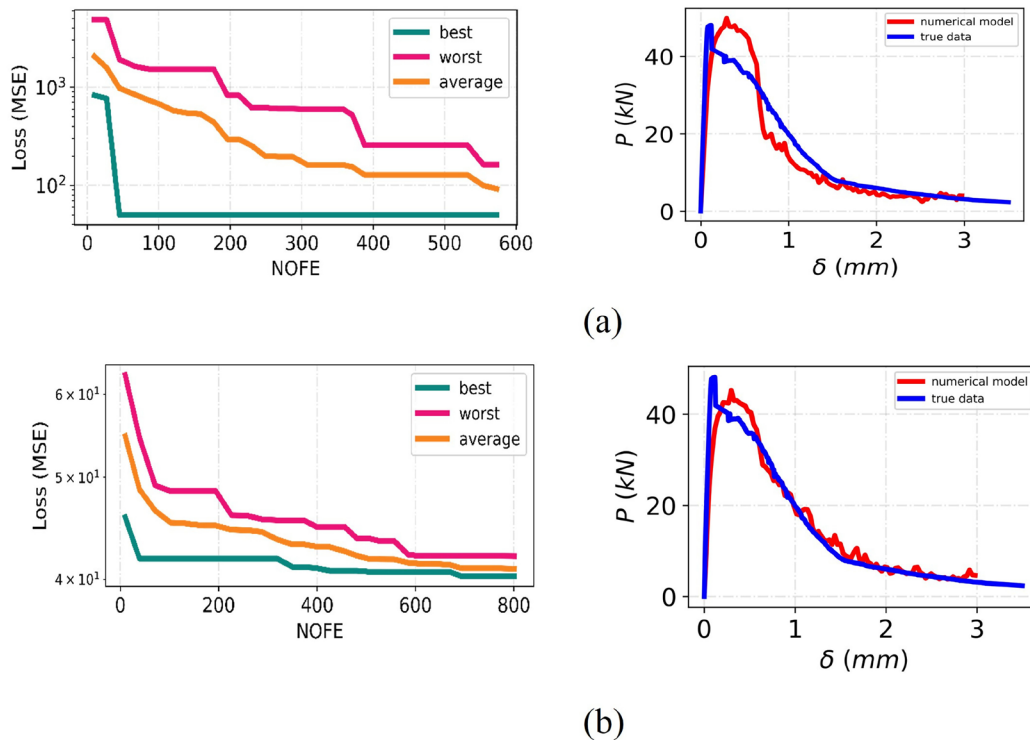


Figure 12: Loss (MSE) versus number of objective function evaluations (NOFE) and load-displacement path for SFRC with 0.5% of fibers: (a) GA results after discrete phase; (b) after fine-tuning phase.

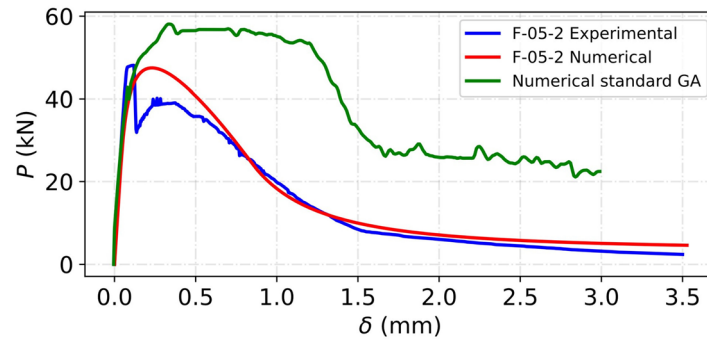


Figure 13: Load-displacement curve by standard GA algorithm optimization and closed-form solution proposed in MOBASHER *et al.* [58] for SFRC with 0.5% of fibers.

Table 9: Best parameters after pipeline optimization.

ALGORITHM	f_{ct1} (MPa)	f_{ct2} (MPa)	ε_2 (mm/mm)	ε_3 (mm/mm)	OF (kN)
GA after discrete phase	2.975	0.606	0.010	0.073	49.84
GA after fine-tuning phase	2.632	0.728	0.009	0.067	40.25

Results after the fine-tuning improve the best solution at 9.59 kN (19.24%). Table 9 presents the design variables identified during optimization analysis. The initial descending branch was not well represented, even though the peak load of the load-deflection curve was well shown, due to the flexural-softening behavior observed in this mixture. The same bad correlation in the initial descending branch was also observed when the closed-form solution proposed in MOBASHER *et al.* [58] was employed (Figure 13). Figure 12(b) shows that the descending branch of the experimental load-deflection curve was best represented after the fine-tuning phase, which was not observed using a conventional inverse optimization process with the standard GA algorithm after 9 hours of processing time (Figure 13).

The tensile strength (f_{ct1}) presented in Table 9 is lower than the experimental tensile strength of the matrix and SFRC with 0.5% of steel fibers presented in Table 2, even though the standard deviation was considered. From the closed-form solution proposed in MOBASHER *et al.* [58], the stresses f_{ct1} and f_{ct2} are 3.03 and 0.15 MPa, respectively, and the strains ε_2 and ε_3 are 0.008 and 0.036, respectively. Therefore, the value obtained from a closed-form solution for stress f_{ct1} is only 15% greater than that obtained from the inverse analysis approach conducted in this paper. However, the value obtained from a closed-form solution for stress f_{ct2} is approximately 80% lower than that obtained from the inverse analysis approach using a finite element method.

It becomes evident that, for SFRC with a flexural-softening behavior, the differences between both inverse analysis approaches are more significant than for SFRC with flexural-hardening behavior. Furthermore, the tensile strength predicted by the inverse analysis approach was 27–39% lower than the experimental value, which indicates that the inverse analysis approach underestimates the tensile strength of SFRC with flexural-softening behavior. This is because fiber-reinforced concrete with flexural-softening behavior presents rotation of the cross-section more restricted to the cracking plane due to the smaller volume of fibers. With the localization of the crack, analytical models or finite element models based on the smeared crack approach tend to overestimate the fracture energy, which was compensated for in the optimization process by the reduction of the tensile strength. It should be noted that the mesh refinement was kept constant in the analysis of the two fiber concrete mixes and that the constitutive law was defined using the stress-strain relationship, without considering the fracture energy of the SFRC.

6. CONCLUSION

This paper proposes a hybrid strategy to automate inverse analysis approaches for deriving the tensile stress-strain relationship of SFRC from beams subjected to four-point loading, which can be used with the finite element method. In addition, two fiber-reinforced concretes with medium-strength concrete (65 MPa), reinforced with 0.5% and 1.5% of hooked-end steel fibers, were developed to validate the proposed inverse analysis approach.

Experimental results showed that SFRC with 1.5% of steel fibers showed flexural-hardening behavior, while SFRC with 0.5% of steel fibers showed flexural-softening behavior. The addition of 1.5% steel fibers

increased the flexural strength of concrete by 28% but did not change the compressive strength or modulus of elasticity. Despite this enhancement in flexural strength, the tensile strength was not influenced by either the addition or increase in the quantity of steel fibers.

All the metaheuristic algorithms compared in this work represented well the load-displacement curve obtained from the bending test under four-point loading. However, the Genetic Algorithm (GA) presented lower mean square error (MSE) when compared to the Simulated Annealing Algorithm (SAA) and Differential Evolution (DE). The MSE measurement for the SFRC with 1.5% of fibers has a value below 10 kN. For the SFRC with 0.5% of fibers, the Genetic Algorithm (GA) showed an MSE of less than 40 kN and is more difficult to represent the load-displacement curve of SFRC with flexural-softening behavior. The higher MSE value for the SFRC with 0.5% of fibers can be explained by the fact that the concrete is more fragile with a lower number of fibers.

The tensile strength predicted by inverse analysis, using all metaheuristic algorithms, agrees well with the experimental results for SFRC with 1.5% of steel fibers. This demonstrates the efficacy of the proposed automated inverse analysis approach using a finite element method for SFRC with flexural-hardening behavior. However, for SFRC with pronounced flexural-softening behavior, the inverse analysis approaches predicted a tensile strength that was 27–39% lower than the experimental value, indicating a localization of the flexural cracking.

The fine-tuning proposed for the optimization pipeline proved necessary for a better fit of the curve obtained from the inverse analysis approach. When this third phase was not used, a greater discrepancy was observed in the force-displacement curve obtained from the test.

The principal limitation of this methodology is its reduced accuracy for SFRC exhibiting pronounced flexural-softening behavior (0.5% fiber content or lower). For this mixture, the model underestimated the experimental tensile strength by 27–39%. This discrepancy is attributed to crack localization, a phenomenon the study's smeared crack finite element approach cannot adequately capture. Consequently, the model is less effective at representing the load-displacement curve for more brittle SFRC composites.

On average, the optimization process required approximately 8 hours to complete a full run and predict the model parameters using the proposed hybrid approach. Although computational efficiency was not the primary objective of this study, future works may explore strategies such as metamodeling or surrogate modeling to reduce computational time and memory usage. These alternatives could facilitate broader parametric analyses and real-time applications in practical engineering scenarios.

Future research will extend the proposed hybrid strategy by applying the automated inverse analysis to determine the tensile stress-strain curves for concretes reinforced with other fiber types, including recycled steel and non-metallic fibers. Furthermore, the optimization pipeline will be integrated with numerical methods more suitable than the Finite Element Method (FEM) with a smeared crack approach, particularly for composites that exhibit pronounced flexural-softening behavior, such as discrete fracture models or the Strong Discontinuity Approach (SDA) models.

7. ACKNOWLEDGMENTS

The authors are thankful for the financial support provided for this research by the Brazilian National Council of Research and Development (CNPq) (projects number: 305622/2023-4 and 305927/2023-0). This study was also financed, in part, by the Coordenação de Aperfeiçoamento de Pessoal de Nível Superior - Brasil (CAPES) - Finance Code 001. The authors also wish to thank the Brazilian companies Belgo Bekaert Arames, MOLD – Estruturas Pré-moldadas, and Votorantin Cimentos, for donating the materials used in the research.

8. BIBLIOGRAPHY

- [1] YANG, J., ZHANG, Y., HUANG, J., “The strengthening theory of steel fiber reinforced concrete and its application in tunnel engineering: a review”, *Journal of Engineered Fibers and Fabrics*, v. 19, pp. 15589250241239242, Jan. 2024. doi: <http://doi.org/10.1177/15589250241239242>.
- [2] PRADEEP KUMAR, C., SHAHUL HAMEED, M., “Experimental study on the behaviour of steel fibre when used as a secondary reinforcement in reinforced concrete beam”, *Materials Today: Proceedings*, v. 52, pp. 1189–1196, 2022. doi: <http://doi.org/10.1016/j.matpr.2021.11.033>.
- [3] LI, N., JIN, Z., LONG, G., *et al.*, “Impact resistance of steel fiber-reinforced self-compacting concrete (SCC) at high strain rates”, *Journal of Building Engineering*, v. 38, pp. 102212, Jun. 2021. doi: <http://doi.org/10.1016/j.jobe.2021.102212>.

- [4] BŁASZCZYŃSKI, T., PRZYBYLSKA-FAŁEK, M., “Steel fibre reinforced concrete as a structural material”, *Procedia Engineering*, v. 122, pp. 282–289, 2015. doi: <http://doi.org/10.1016/j.proeng.2015.10.037>.
- [5] WANG, X., FAN, F., LAI, J., *et al.*, “Steel fiber reinforced concrete: a review of its material properties and usage in tunnel lining”, *Structures*, v. 34, pp. 1080–1098, Dec. 2021. doi: <http://doi.org/10.1016/j.istruc.2021.07.086>.
- [6] AHMAD, I., SHOKOUHIAN, M., “Promoting sustainable green infrastructure: experimental and numerical investigation of concrete reinforced with recycled steel fibers”, *Archives of Advanced Engineering Science*, pp. 1–13, Jun. 2024. doi: <http://doi.org/10.47852/bonviewAAES42022837>.
- [7] HOANG, N.-D., “Predicting tensile strength of steel fiber-reinforced concrete based on a novel differential evolution-optimized extreme gradient boosting machine”, *Neural Computing & Applications*, v. 36, n. 36, pp. 22653–22676, Sep. 2024. doi: <http://doi.org/10.1007/s00521-024-10458-x>.
- [8] NOUR, A., MASSICOTTE, B., DE MONTAIGNAC, R., *et al.*, “Development of an inverse analysis procedure for the characterisation of softening diagrams for FRC beams and panels”, *Construction & Building Materials*, v. 94, pp. 35–44, Sep. 2015. doi: <http://doi.org/10.1016/j.conbuildmat.2015.06.049>.
- [9] AFSHARI, E., MOSSAIBY, F., BAKHSHPOORI, T., “Metaheuristic-based crack detection in beam-type structures using peridynamics theory: a comparative study”, *Mechanics of Advanced Materials and Structures*, v. 31, n. 13, pp. 2844–2858, Jul. 2024. doi: <http://doi.org/10.1080/15376494.2023.2164911>.
- [10] KHOSO, S., RAAD, J., PARVIN, A., “State of the art review on the properties of sustainable concrete using hybrid fibers”, *International Journal of Energy, Environment and Ecology*, v. 30, n. 1, pp. 37–52, 2023.
- [11] ORTIZ NAVAS, F., NAVARRO-GREGORI, J., CONFORTI, A., *et al.*, “State-of-the-Art review of synthetic fibres as shear reinforcement in concrete elements”, *Hormigón y Acero*, v. 75, n. 302-303, pp. 147–156, Mar. 2023. doi: <http://doi.org/10.33586/hya.2023.3106>.
- [12] VAIRAGADE, V.S., DHALE, S.A., “Hybrid fibre reinforced concrete: a state of the art review”, *Hybrid Advances*, v. 3, pp. 100035, Aug. 2023. doi: <http://doi.org/10.1016/j.hybadv.2023.100035>.
- [13] SHAFEL, B., KAZEMIAN, M., DOPKO, M., *et al.*, “State-of-the-Art review of capabilities and limitations of polymer and glass fibers used for fiber-reinforced concrete”, *Materials*, v. 14, n. 2, pp. 409, Jan. 2021. doi: <http://doi.org/10.3390/ma14020409>. PubMed PMID: 33467581.
- [14] AMERICAN CONCRETE INSTITUTE, *ACI 544.8R-16: Report on indirect method to obtain stress-strain response of fiber-reinforced concrete (FRC)*, Michigan, American Concrete Institute, 2016.
- [15] CARVALHO, P.P.M.D., LAMEIRAS, R.D.M., “A simplified inverse analysis procedure for the stress-crack opening relationship of fiber-reinforced concrete”, *Buildings*, v. 13, n. 5, pp. 1166, Apr. 2023. doi: <http://doi.org/10.3390/buildings13051166>.
- [16] BARROS, J.A.O., CRUZ, J.S., “Fracture energy of steel fiber-reinforced concrete”, *Mechanics of Composite Materials and Structures*, v. 8, n. 1, pp. 29–45, Jan. 2001. doi: <http://doi.org/10.1080/107594101459815>.
- [17] TLEMAT, H., PILAKOUTAS, K., NEOCLEOUS, K., “Modelling of SFRC using inverse finite element analysis”, *Materials and Structures*, v. 39, n. 2, pp. 221–233, 2006. doi: <http://doi.org/10.1617/s11527-005-9010-y>.
- [18] MATOS, L.M.P., BARROS, J.A.O., VENTURA-GOUVEIA, A., *et al.*, “A new inverse analysis approach for predicting the fracture mode I parameters of fibre reinforced concrete”, *Engineering Fracture Mechanics*, v. 246, pp. 107613, Apr. 2021. doi: <http://doi.org/10.1016/j.engfracmech.2021.107613>.
- [19] SORANAKOM, C., MOBASHER, B., “Correlation of tensile and flexural responses of strain softening and strain hardening cement composites”, *Cement and Concrete Composites*, v. 30, n. 6, pp. 465–477, Jul. 2008. doi: <http://doi.org/10.1016/j.cemconcomp.2008.01.007>.
- [20] WARDEH, M.A., TOUTANJI, H.A., “Parameter estimation of an anisotropic damage model for concrete using genetic algorithms”, *International Journal of Damage Mechanics*, v. 26, n. 6, pp. 801–825, Aug. 2017. doi: <http://doi.org/10.1177/1056789515622803>.
- [21] MAGACHO, E.G., JORGE, A.B., GOMES, G.F., “Inverse problem based multiobjective sunflower optimization for structural health monitoring of three-dimensional trusses”, *Evolutionary Intelligence*, v. 16, n. 1, pp. 247–267, Feb. 2023. doi: <http://doi.org/10.1007/s12065-021-00652-4>.
- [22] CAO, P., ZHANG, Y., ZHOU, K., *et al.*, “A reinforcement learning hyper-heuristic in multi-objective optimization with application to structural damage identification”, *Structural and Multidisciplinary Optimization*, v. 66, n. 1, pp. 16, Jan. 2023. doi: <http://doi.org/10.1007/s00158-022-03432-5>.

- [23] MANIE, J., KIKSTRA, W.P., *Diana User's manual release 10.1*, Haia, DIANA FEA BV, 2017.
- [24] PELTERET, J.-P., WALTER, B., STEINMANN, P., "Application of metaheuristic algorithms to the identification of nonlinear magneto-viscoelastic constitutive parameters", *Journal of Magnetism and Magnetic Materials*, v. 464, pp. 116–131, Oct. 2018. doi: <http://doi.org/10.1016/j.jmmm.2018.02.094>.
- [25] NAIT AMAR, M., JAHANBANI GHAFAROKHI, A., NG, C.S.W., *et al.*, "Optimization of WAG in real geological field using rigorous soft computing techniques and nature-inspired algorithms", *Journal of Petroleum Science Engineering*, v. 206, pp. 109038, Nov. 2021. doi: <http://doi.org/10.1016/j.petrol.2021.109038>.
- [26] NG, C.S.W., NAIT AMAR, M., JAHANBANI GHAFAROKHI, A., *et al.*, "A survey on the application of machine learning and metaheuristic algorithms for intelligent proxy modeling in reservoir simulation", *Computers & Chemical Engineering*, v. 170, pp. 108107, Feb. 2023. doi: <http://doi.org/10.1016/j.compchemeng.2022.108107>.
- [27] KAZEMI, F., ASGARKHANI, N., SHAFIGHFARD, T., *et al.*, "Machine-learning methods for estimating performance of structural concrete members reinforced with fiber-reinforced polymers", *Archives of Computational Methods in Engineering*, v. 32, n. 1, pp. 571–603, Jan. 2025. doi: <http://doi.org/10.1007/s11831-024-10143-1>.
- [28] SHAFIGHFARD, T., KAZEMI, F., ASGARKHANI, N., *et al.*, "Machine-learning methods for estimating compressive strength of high-performance alkali-activated concrete", *Engineering Applications of Artificial Intelligence*, v. 136, pp. 109053, Oct. 2024. doi: <http://doi.org/10.1016/j.engappai.2024.109053>.
- [29] AZEVEDO, B.F., ROCHA, A.M.A.C., PEREIRA, A.I., "Hybrid approaches to optimization and machine learning methods: a systematic literature review", *Machine Learning*, v. 113, n. 7, pp. 4055–4097, Jul. 2024. doi: <http://doi.org/10.1007/s10994-023-06467-x>.
- [30] KATOCH, S., CHAUHAN, S.S., KUMAR, V., "A review on genetic algorithm: past, present, and future", *Multimedia Tools and Applications*, v. 80, n. 5, pp. 8091–8126, Feb. 2021. doi: <http://doi.org/10.1007/s11042-020-10139-6>. PubMed PMID: 33162782.
- [31] GOEL, L., KANHAR, J., PATEL, V.S., *et al.*, "Hybrid elephant herding optimization–big bang big crunch for pattern recognition from natural images", *Soft Computing*, v. 28, n. 4, pp. 3431–3447, Feb. 2024. doi: <http://doi.org/10.1007/s00500-023-08667-y>.
- [32] MAHAJAN, G., CHAUDHARY, N., "Design and development of novel hybrid optimization-based convolutional neural network for software bug localization", *Soft Computing*, v. 26, n. 24, pp. 13651–13672, Dec. 2022. doi: <http://doi.org/10.1007/s00500-022-07341-z>.
- [33] PEREIRA JUNIOR, W.M., ARAÚJO, D.L., PITUBA, J.J.C., "Numerical analysis of steel-fiber-reinforced concrete beams using damage mechanics", *Revista IBRACON de Estruturas e Materiais*, v. 9, n. 2, pp. 153–191, Apr. 2016. doi: <http://doi.org/10.1590/S1983-41952016000200002>.
- [34] BLASI, G., LEONE, M., "Inverse analysis-based model for the tensile behaviour of fibre-reinforced concrete with manufactured and waste tyres recovered fibres", *Case Studies in Construction Materials*, v. 17, pp. e01297, Dec. 2022. doi: <http://doi.org/10.1016/j.cscm.2022.e01297>.
- [35] HOLLAND, J.H., *Adaptation in natural and artificial systems: an introductory analysis with applications to biology, control, and artificial intelligence*, Cambridge, MIT Press, 1992. doi: <http://doi.org/10.7551/mitpress/1090.001.0001>.
- [36] MASOUMI, M., MASOUMI, M., JAMSHIDI, E., "Damage diagnosis in steel structures with different noise levels via optimization algorithms", *International Journal of Steel Structures*, v. 15, n. 3, pp. 557–565, 2015. doi: <http://doi.org/10.1007/s13296-015-9004-8>.
- [37] TAVAKOLPOUR, A.R., MAT DARUS, I.Z., TOKHI, O., *et al.*, "Genetic algorithm-based identification of transfer function parameters for a rectangular flexible plate system", *Engineering Applications of Artificial Intelligence*, v. 23, n. 8, pp. 1388–1397, Dec. 2010. doi: <http://doi.org/10.1016/j.engappai.2010.01.005>.
- [38] ALHADDAD, W., HALABI, Y., MEREE, H., *et al.*, "Optimum design method for simplified model of outrigger and ladder systems in tall buildings using genetic algorithm", *Structures*, v. 28, pp. 2467–2487, Dec. 2020. doi: <http://doi.org/10.1016/j.istruc.2020.09.066>.
- [39] KRAMER, O., *Genetic algorithm essentials*, v. 679, Cham, Springer International Publishing, 2017. doi: <http://doi.org/10.1007/978-3-319-52156-5>.
- [40] AL-BETAR, M.A., "β-Hill climbing: an exploratory local search", *Neural Computing & Applications*, v. 28, n. S1, pp. 153–168, Dec. 2017. doi: <http://doi.org/10.1007/s00521-016-2328-2>.

- [41] KIRKPATRICK, S., GELATT JUNIOR, C.D., VECCHI, M.P., “Optimization by simulated annealing”, *Science*, v. 220, n. 4598, pp. 671–680, May. 1983. doi: <http://doi.org/10.1126/science.220.4598.671>. PubMed PMID: 17813860.
- [42] METROPOLIS, N., ROSENBLUTH, A.W., ROSENBLUTH, M.N., *et al.*, “Equation of state calculations by fast computing machines”, *The Journal of Chemical Physics*, v. 21, n. 1087, pp. 1–7, 1953.
- [43] STORN, R., PRICE, K., “Differential Evolution: a simple and efficient heuristic for global optimization over continuous spaces”, *Journal of Global Optimization*, v. 11, n. 4, pp. 341–359, 1997. doi: <http://doi.org/10.1023/A:1008202821328>.
- [44] BILAL, PANT, M., ZAHEER, H., *et al.*, “Differential Evolution: a review of more than two decades of research”, *Engineering Applications of Artificial Intelligence*, v. 90, pp. 103479, Apr. 2020. doi: <http://doi.org/10.1016/j.engappai.2020.103479>.
- [45] WU, G., SHEN, X., LI, H., *et al.*, “Ensemble of differential evolution variants”, *Information Sciences*, v. 423, pp. 172–186, Jan. 2018. doi: <http://doi.org/10.1016/j.ins.2017.09.053>.
- [46] ARAÚJO, D.D.L., LOBO, F.A., MARTINS, B.G., “A shear stress-slip relationship in steel fibre-reinforced concrete obtained from push-off testing”, *Construction & Building Materials*, v. 293, pp. 123435, Jul. 2021. doi: <http://doi.org/10.1016/j.conbuildmat.2021.123435>.
- [47] ASSOCIAÇÃO BRASILEIRA DE NORMAS TÉCNICAS, *ABNT NBR 5739: Concreto - Ensaio de Compressão de Corpos de Prova Cilíndricos*, Rio de Janeiro, ABNT, 2018.
- [48] ASSOCIAÇÃO BRASILEIRA DE NORMAS TÉCNICAS, *ABNT NBR 8522 - Concreto endurecido - Determinação dos Módulos de Elasticidade e de Deformação. Parte 1: Módulos Estáticos à Compressão*, Rio de Janeiro, ABNT, 2021.
- [49] AMERICAN SOCIETY FOR TESTING AND MATERIALS, *ASTM C1609/C1609M-12: Standard Test Method for Flexural Performance of Fiber-Reinforced Concrete (Using Beam With Third-Point Loading)*, West Conshohocken, ASTM, 2019.
- [50] FÉDÉRATION INTERNATIONALE DU BÉTON, *Model code for concrete structures*, Lausanne, FIB, 2010.
- [51] PEREIRA JUNIOR, W.M., BORGES, R.A., ARAÚJO, D.L., *et al.*, “Parametric identification and sensitivity analysis combined with a damage model for reinforced concrete structures”, *Arabian Journal for Science and Engineering*, Aug. 2022.
- [52] PEREIRA JUNIOR, W.M., BORGES, R.A., ARAÚJO, D.L., *et al.*, “A proposal to use the inverse problem for determining parameters in a constitutive model for concrete”, *Soft Computing*, v. 25, n. 13, pp. 8797–8815, Jul. 2021. doi: <http://doi.org/10.1007/s00500-021-05745-x>.
- [53] HODSON, T.O., OVER, T.M., FOKS, S.S., “Mean squared error, deconstructed”, *Journal of Advances in Modeling Earth Systems*, v. 13, n. 12, pp. e2021MS002681, Dec. 2021. doi: <http://doi.org/10.1029/2021MS002681>.
- [54] DUPONT, D., “Modelling and experimental validation of the constitutive law (σ - ϵ) and cracking behaviour of steel fiber reinforced concrete”, M.Sc. Thesis, Catholic University of Leuven, Leuven, 2003.
- [55] BAŽANT, Z.P., OH, B.H., “Crack band theory for fracture of concrete”, *Materiales de Construcción*, v. 16, n. 3, pp. 155–177, May. 1983.
- [56] ČERVENKA, J., ČERVENKA, V., LASERNA, S., “On crack band model in finite element analysis of concrete fracture in engineering practice”, *Engineering Fracture Mechanics*, v. 197, pp. 27–47, Jun. 2018. doi: <http://doi.org/10.1016/j.engfracmech.2018.04.010>.
- [57] SHI, X., PARK, P., REW, Y., *et al.*, “Constitutive behaviors of steel fiber reinforced concrete under uniaxial compression and tension”, *Construction & Building Materials*, v. 233, pp. 117316, Feb. 2020. doi: <http://doi.org/10.1016/j.conbuildmat.2019.117316>.
- [58] MOBASHER, B., YAO, Y., SORANAKOM, C., “Analytical solutions for flexural design of hybrid steel fiber reinforced concrete beams”, *Engineering Structures*, v. 100, pp. 164–177, Oct. 2015. doi: <http://doi.org/10.1016/j.engstruct.2015.06.006>.